Investigation of laser-induced cell lysis using time-resolved imaging

Kaustubh R. Rau and Arnold Guerra III
Laser Microbeam and Medical Program, Beckman Laser Institute, University of California, Irvine, Irvine, California 92697

Alfred Vogel
Medical Laser Center Lübeck, Peter Monnik Weg 4, D23562, Lübeck, Germany

Vasan Venugopalan[a)]
Departments of Chemical Engineering & Materials Science and Biomedical Engineering and Laser Microbeam and Medical Program, Beckman Laser Institute, University of California, Irvine, Irvine, California 92697

(Received 21 July 2003; accepted 19 February 2004)

Using time-resolved imaging, we investigated the lysis of confluent PtK2 cell cultures by pulsed laser microbeam irradiation. Images obtained at time delays of 0.5 ns to 50 μs demonstrate lysis to be mediated by laser-induced plasma formation resulting in pressure wave propagation and cavitation bubble formation. Image analysis enabled quantitative characterization of the pressure wave and cavitation bubble dynamics. The zone of cell damage exceeded the plasma size and serves to implicate cavitation bubble expansion as the primary agent of cell injury. © *2004 American Institute of Physics.* [DOI: 10.1063/1.1705728]

Highly focused laser microbeams with femtosecond to nanosecond pulse durations are used increasingly for targeted cell lysis,[1] microsurgery of cellular structures,[2] sampling of cellular contents for biochemical analysis,[3,4] and molecular delivery via transient permeabilization of the plasma cell membrane.[5–7] Recently, Venugopalan and coworkers examined optical breakdown (plasma formation) in pure water produced by 6 ns laser pulses at $\lambda=532$ and 1064 nm when focused at high numerical aperture (NA).[8] They showed that the laser parameters used to produce cell lysis as well as transient cell membrane permeabilization are sufficient to produce optical breakdown.[5] Based on these results, they concluded that laser-induced plasma formation is the mechanism driving a broad range of laser-based cellular micromanipulation techniques.

In this study, we examined the physical mechanisms governing laser-induced cell lysis by imaging potorous rat kidney epithelial (PtK2) cell cultures following the delivery of a 6 ns pulse (FWHM) from a $\lambda=532$ nm Nd:YAG laser (Brilliant B, Quantel Inc.) focused at high NA. The resulting plasma formation, pressure wave propagation, and cavitation bubble dynamics were imaged at delay times spanning five orders of magnitude (0.5 ns–50 μs). The laser output was introduced via the epifluorescence port of an inverted microscope (Zeiss Axiovert S100) into the back aperture of the microscope objective. A bright-field (40×; 0.8 NA, Zeiss Achroplan) or phase-contrast (40×, 0.65 NA, ph2, Zeiss A-Plan) objective was used to both visualize the cells and deliver the laser radiation. PtK2 cells were cultured in phenol red free medium transparent to 532 nm radiation. Cells were grown in Petri dishes with a glass cover slide window for microscope examination.

Time resolved images were acquired by a gated intensified CCD camera (PI-MAX, Roper Scientific) triggered at specific delay times following the arrival of the Nd:YAG laser pulse. A filter (LP 570, Edmund Optics) was used to prevent scattered laser radiation from reaching the camera. Imaging was enabled by transilluminating the sample at the desired time delay. For delays <1 μs, we used a dye cell pumped by a split-off portion of the 532 nm laser pulse. The dye fluorescence (LDS 698, Exciton Inc) was 15 ns in duration and coupled into a multimode optical fiber whose length determined the time delay for illumination. For delays >1 μs, we used an electronically triggered flash lamp (Nanolite KL-L, High-Speed Photo Systeme) with a 40 ns duration. Images acquired at delays <1 μs were taken using a camera gate width of 0.5 ns while images taken at larger delay times employed a 200 ns gate width. The short gate width provided clear images without averaging and enabled measurement of pressure wave and cavitation bubble dynamics with improved accuracy compared to previous studies.[8,9] While optical breakdown in water[9,10] and selective targeting of cells loaded with light-absorbing micro- and nano-particles[11] have been imaged, this letter provides time-resolved visualization and analysis of cell lysis produced by laser-induced plasma formation.

The threshold for plasma formation in the cell culture, i.e., the pulse energy providing a 50% probability for optical breakdown, was 8 μJ. The observation of plasma luminescence was taken as evidence of optical breakdown. We examined cell lysis at pulse energies corresponding to 1× and 3× threshold. No cellular effects were observed in the absence of plasma formation. In an earlier study, we measured a plasma threshold of 1.9 μJ using a cuvette that allowed the immersion of a 0.9 NA objective in distilled water. The higher threshold found here is due to the use of a lower NA objective combined with optical aberrations introduced by epi-fluorescence lamp conditioning optics, a dichroic beamsplitter, and a glass coverslip that lie in the path of the laser

[a)]Author to whom correspondence should be addressed; electronic mail: vvenugop@uci.edu

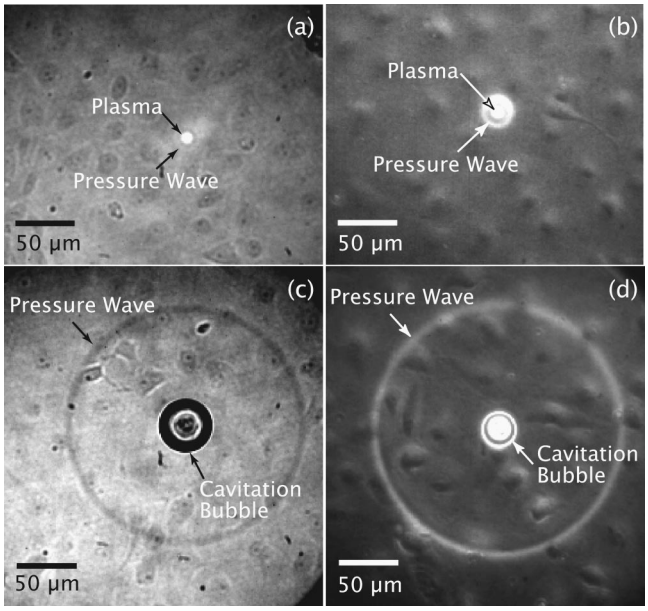

FIG. 1. Laser-induced breakdown in PtK2 cell culture at time delays of (a), (b) 10 ns and (c), (d) 67 ns visualized using (a), (c) bright-field and (b), (d) phase-contrast microscopy.

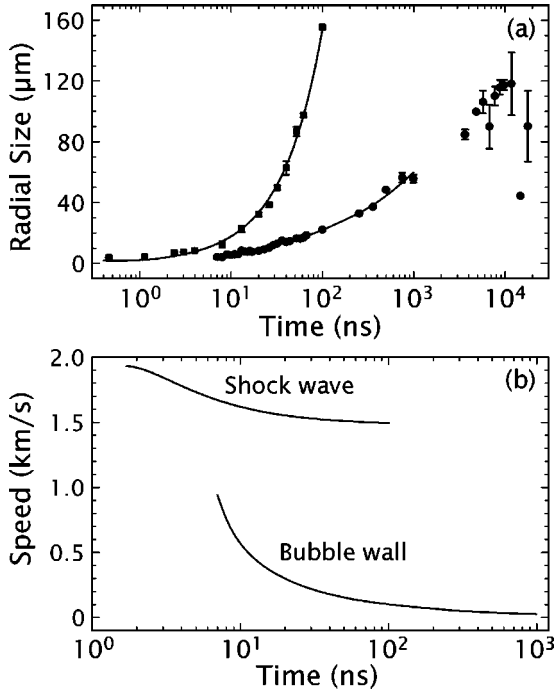

FIG. 2. (a) Position and (b) speed of pressure wave propagation (■) and cavitation bubble rim (●) at 1× threshold. The curves in (a) represent the data fits used to determine the speeds shown in (b).

beam when using a conventional microscope system.[12]

Figure 1 shows typical time-resolved images using bright-field [Figs. 1(a) and 1(c)] and phase-contrast (Figs. 1(b) and 1(d)] objectives. The maximum plasma size is reached at 20 ns and the pressure wave resulting from the plasma expansion is clearly seen in Figs. 1(a) and 1(b). At 67 ns [Figs. 1(c) and 1(d)], the cavitation bubble resulting from the plasma expansion is visible and the pressure wave has propagated outwards. In Fig. 1(c), the outer portions of the cavitation bubble appear dark due to the reflection of the illumination by the curved bubble surface. However, light can pass through the bubble center and cellular damage is clearly visible in this region. While phase-contrast imaging provides better visualization of the PtK2 cells and the shock wave, the region beneath the cavitation bubble surface is obscured.

Figure 2(a) provides the radial size of the pressure wave and bubble rim versus time at threshold. Each data point represents the average and standard deviation of three images. Figure 2(b) presents the speeds of the pressure wave $u_s(t)$ and bubble rim $u_B(t)$ as determined by the derivative of the data fits shown in Fig. 2(a). At early times the pressure wave is supersonic with maximum speeds approaching 2000 m/s for both 1× and 3× (not shown) threshold; i.e., it is a shock wave. These shock waves decay to sonic speed within 100 ns. The bubble wall speeds are plotted once the bubble rim is clearly distinguished from the shock wave and possess maximum values of 940 and 1070 m/s at 1× and 3× threshold, respectively.

The shock wave amplitudes p_s were obtained from the pressure wave speeds using the following relation:[9]

$$p_s = C_1 \rho_0 u_s [10^{(u_s - c_0)/C_2} - 1], \tag{1}$$

where $\rho_0 = 998$ kg/m^3 is the density of water, $c_0 = 1483$ m/s is the speed of sound in water, $C_1 = 5190$ m/s, and $C_2 = 25\,306$ m/s. These results are shown in Fig. 3 and reveal maximum pressures of 420–460 MPa which decay rapidly as the shock wave propagates.

Figure 4(a) is an image taken 5 μs after laser irradiation at 3× threshold showing the large cavitation bubble produced by the breakdown process. The maximum bubble diameter D_B was determined from the images and used to calculate the bubble energy E_B using the following relation:[9]

$$E_B = \tfrac{1}{12}\pi D_B^3 (p_\infty - p_v), \tag{2}$$

where p_∞ is atmospheric pressure and p_v is the vapor pressure within the expanded bubble (2330 Pa at 20 °C). Table I provides values for E_B and D_B, along with the laser pulse energy E_p, the diameter of the cell lysis region D_{lys}, and the maximum plasma size D_{pl}. The data show that a significant fraction of the laser pulse energy is converted to bubble energy. The cell lysis region, as shown in Fig. 4(b), is defined as the area denuded of cells surrounding the irradiation site and is much smaller than the maximum cavitation bubble size. Specifically, $D_{\text{lys}} = 44$ and 80 μm for 1× and 3× threshold, respectively, while the corresponding maximum

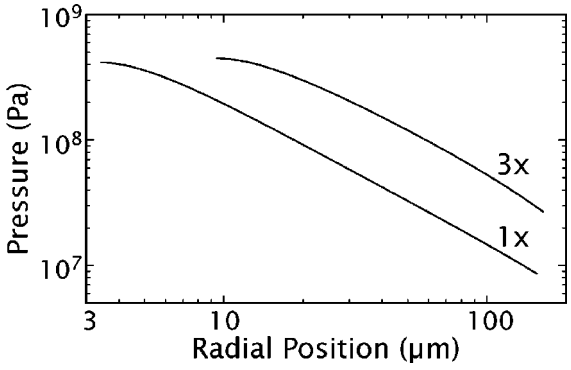

FIG. 3. Shock wave pressures at 1× and 3× threshold.

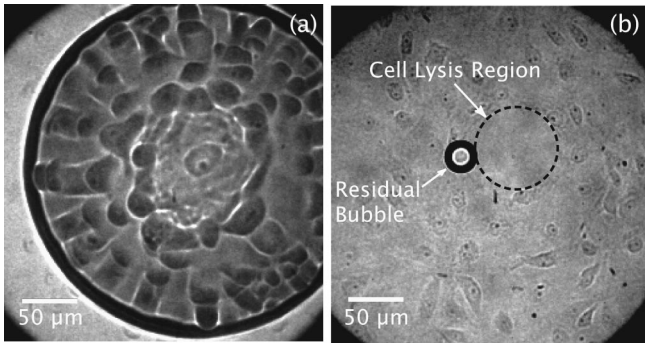

FIG. 4. (a) Cavitation bubble shown at 5 μs at 3× threshold. The lysis zone and deformed cells are clearly visible. (b) PtK2 cell sample post-irradiation. A residual bubble is often produced when irradiating at larger pulse energies.

bubble diameters are 240 and 440 μm. Moreover, Fig. 4(a) shows that the later stages of bubble expansion produce considerable deformation of the cells surrounding lysis region as evidenced by their ''bulging'' away from the irradiation site. However, fluorescent dye assays evaluating acridine orange uptake and propidium iodide exclusion immediately after irradiation and further examination after 24 h revealed that nearly all of these cells have intact membranes and are viable. Thus, the viable PtK2 cells neighboring the denuded area survive the deformation produced by shear stress associated with the fluid flow around the cavitation bubble as well as exposure to shock wave pressures of 50–120 MPa. A study of cell deformation induced by ultrasound contrast agent bubbles came to similar conclusions regarding the ability of cells to survive cavitation bubble dynamics.[13] However, a study on corneal endothelial cells showed that cell death was produced in a relatively large region around the denuded area.[14]

Close examination of our images reveals the lysis region to be fully developed within 1 μs, i.e., during the bubble expansion. This is consistent with a recent theoretical analysis of cell deformation resulting from shock wave passage and cavitation bubble dynamics in extracorporeal shockwave lithotripsy.[15] Application of this analysis to our situation reveals that the hydrodynamic stresses associated with the fluid flow driven by the expanding cavitation bubble is primarily responsible for cell lysis. Moreover, we found that the border of the cell lysis region is specified by the location at which the product of the transient shear stress and the characteristic bubble expansion time falls below a critical value; implying that cell lysis is sensitive to both the stress amplitude and its duration.

TABLE I. Laser pulse energy E_p, bubble energy E_B, maximum bubble diameter D_B, diameter of cell lysis D_{lys}, and maximum plasma size D_{pl} at 1× and 3× threshold.

	E_p (μJ)	E_B (μJ)	D_B (μm)	D_{lys} (μm)	D_{pl} (μm)
1× threshold	8	0.36	240	44	7.2
3× threshold	24	2.2	440	80	16.2

The authors acknowledge support from the National Institutes of Health via the Laser Microbeam and Medical Program (P41-RR-01192) and Bioengineering Research Partnership Program (R01-EB-00313).

[1] K. Schütze, H. Pösl, and G. Lahr, Cell Mol. Biol. (Paris) **44**, 735 (1998).
[2] A. Khodjakov, R. W. Cole, B. R. Oakley, and C. L. Rieder, Curr. Biol. **10**, 59 (2000).
[3] K. Schütze and G. Lahr, Nature Biotech. **16**, 737 (1998).
[4] H. Li, C. E. Sims, H. Y. Wu, and N. L. Allbritton, Anal. Chem. **73**, 4625 (2001).
[5] T. B. Krasieva, C. F. Chapman, V. J. LaMorte, V. Venugopalan, M. W. Berns, and B. J. Tromberg, Proc. SPIE **3260**, 38 (1998).
[6] J. S. Soughayer, T. Krasieva, S. C. Jacobsen, J. M. Ramsey, B. J. Tromberg, and N. L. Allbritton, Anal. Chem. **72**, 1342 (2000).
[7] U. K. Tirlapur and K. König, Nature (London) **418**, 290 (2002).
[8] V. Venugopalan, A. Guerra III, K. Nahen, and A. Vogel, Phys. Rev. Lett. **88**, 078103 (2002).
[9] A. Vogel, S. Busch, and U. Parlitz, J. Acoust. Soc. Am. **100**, 148 (1996).
[10] C. B. Schaffer, N. Nishimura, E. N. Glezer, A. M.-T. Kim, and E. Mazur, Opt. Express **10**, 196 (2002).
[11] C. M. Pitsillides, E. K. Joe, X. Wei, R. R. Anderson, and C. P. Lin, Biophys. J. **84**, 4023 (2003).
[12] A. Vogel, K. Nahen, D. Theisen, R. Birngruber, R. J. Thomas, and B. Rockwell, Appl. Opt. **38**, 3636 (1999).
[13] B. Wolfrum, R. Mettin, T. Kurz, and W. Lauterborn, Appl. Phys. Lett. **81**, 5060 (2002).
[14] A. Vogel, P. Schweiger, A. Frieser, M. N. Asiyo, and R. Birngruber, IEEE J. Quantum Electron. **26**, 2240 (1990).
[15] M. Lokhandwalla and B. Sturtevant, Phys. Med. Biol. **46**, 413 (2001).